ASYMMETRIC B FACTORIES

FERNANDO MARTíNEZ-VIDAL
IN2P3-CNRS/Universités Paris 6 & 7, France
E-mail: martinef@SLAC.Stanford.EDU

After more than a decade of preparation, a new race of experiments known as Asymmetric B Factories, were commissioned in early 1999 and started operation before the fall of the year. Asymmetric B Factories are expected to largely improve our knowledge of one of the currently most exciting mysteries in Particle Physics with major consequences on Cosmology: the origin and nature of CP violation. The Physics motivation and the basics of those experiments, as well as the initial performances and early results are reported in this talk.

1 Introduction

According to the Big Bang theory, matter and antimatter existed in equal amounts when the Universe was a fraction of nanosecond old. Almost all these particles and antiparticles quickly disappeared in a blaze of mutual annihilation. Only about one in about one billion particles survived. The rest ended up as photons in the cosmic background radiation. Why did the matter not annihilate completely with antimatter inmediately after its creation? Could be an equal matter and antimatter scapes from the blaze. Astrophysicists have searched for antimatter galaxies and even larger structures by looking for the violent matter annihilation activity that would occur at their boundaries. But no such structures have been identified so far, up to extremely large scales of billions of light years. Therefore we seem to live in an Universe largely dominated by matter. These facts lead us one of the most exciting mysteries of the Universe: the matter/antimatter asymmetry.

According to our model of fundamental interactions, the combined operations of C (charge conjugation) and P (parity) take matter into anti-matter [1]. CP violating processes could then provide an absolute distinction between matter and antimatter. In 1964, Cronin *et al.* at Brookheaven discovered a tiny but non-zero violation of the CP symmetry in the $K^0\bar{K}^0$ system [2]. In 1967, Andrei Sakharov conceived a mechanism by which a tiny excess of matter over antimatter could arise in the early Universe [3]. In his idea, CP violation, as well as the baryon number violation and C violation in an expanding Universe (with deviations from thermal equilibrium), is an essential ingredient to generate the Baryon Asymmetry of the Universe (BAU). It was thought that BAU could only be generated at the scale of the Grand Unification [4]. However, in 1985 it was realized that the electroweak transition

[5] could have dramatic consequences on any baryon asymmetry generated at higher temperature, and could be at the origin of the observed number of baryon to photon ratio [6] ($n_b/n_\gamma \sim 10^{-9} - 10^{-10}$). The possibility to generate CP violation at the electroweak scale makes the study of the Standard Model (SM) "scenario" [7] (for which we have definite predictions) extremely exciting. However, it seems very difficult to produce large enough BAU at the electroweak scale [8], at least in the minimal SM with one scalar Higgs doublet. Therefore, one is tempted to predict other sources of CP violation at larger scales and thus a comprehensive study of this phenomenon is of crucial importance.

Almost 40 years after the observation of CP violation in the neutral kaon system, the understanding of this effect has made big progress, and it has been observed in several decays [9], but all of them involve K^0 particles. Therefore there is no evidence so far that this phenomenon is indeed a fundamental property of the weak interactions: CP violation is today one of the least constrained subjects in High Energy Physics.

The existence of the third generation of fermions was originally predicted to accommodate CP violation into the SM via a non-trivial phase of the quark mixing matrix [10]. The coupling between up- and down- type quarks is described by the CKM matrix:

$$V_{CKM} = \begin{pmatrix} V_{ud} & V_{us} & V_{ub} \\ V_{cd} & V_{cs} & V_{cb} \\ V_{td} & V_{ts} & V_{tb} \end{pmatrix} \tag{1}$$

Unitarity implies that the matrix can be described using four independent parameters: the convenient Wolfenstein parameterization [11] involves expanding in terms of $\lambda = \sin\theta_C = 0.2205 \pm 0.0018$ [12]:

$$V_{CKM} = \begin{pmatrix} 1-\lambda^2/2 & \lambda & A\lambda^3(\rho - i\eta) \\ -\lambda & 1-\lambda^2/2 & A\lambda^2 \\ A\lambda^3(1-\rho-i\eta) & V_{ts} & 1 \end{pmatrix} + \mathcal{O}(\lambda^4) \tag{2}$$

$A = 0.80 \pm 0.04$ [12] can be determined from the measurement of $\mid V_{cb} \mid$ in semileptonic decays [12], leaving two parameters to be determined: ρ and η; the latter describes the imaginary part of the matrix, and $\eta \neq 0$ corresponds to the existence of CP violation. One of the unitarity conditions is particularly interesting: $V_{ud}V_{ub}^* + V_{cd}V_{cb}^* + V_{td}V_{tb}^* = 0$, which corresponds to a triangle (with sides of similar length, $\sim A\lambda^3$) relationship in the (ρ, η) plane, illustrated in Fig. 1 (after normalization by λV_{cb}). Constraints on the triangle's apex can be found from a fit to data for $\mid V_{ub}/V_{cb} \mid$,

$$\rho^2 + \eta^2 \propto \Gamma_{b\to u\ell\bar{\nu}} \tag{3}$$

which measures the length of one of the sides, and $\mid V_{td} \mid$ extracted from the frequency for $B^0_d \bar{B}^0_d$ oscillations, Δm_d,

$$(1-\rho)^2 + \eta^2 \propto \Delta m_d \ , \tag{4}$$

which measures the length of another side. The main source of uncertainty on the extraction of $\mid V_{td} \mid$ from $B^0 \overline{B}^0$ oscillations is due to the rather large theoretical uncertainties on QCD matrix element calculations [13]. Reducing this uncertainty is possible by measuring Δm_s (actually imposing limits) from $B^0_s \bar{B}^0_s$ oscillations, and applying constraints on the ratio $\mid V_{td} \mid / \mid V_{ts} \mid$ [14]. The third side of the triangle is unity by construction. The kaon CP violation parameter ϵ_K [9] also provides a hyperbolic constraint on the apex, assuming that observed CP violation in the neutral kaon system is due to the SM. Nevertheless, quantitative tests of the SM using kaons are limited due to the presence of large hadronic effects, very difficult to predict. The angles of the triangle,

$$\arg V_{td} = -\beta = \tan^{-1} \frac{\eta}{1-\rho} \ , \qquad \arg V_{ub} = -\gamma = \tan^{-1} \frac{\eta}{\rho} \ , \tag{5}$$

are directly related to CP asymmetries in B decays, so their measurement would allow a stringent test of the SM. Our current knowledge of the triangle is rather poor [12].

Regardless any particular model, CP violating effects in B decays can be generated by three different possible mechanisms and might be observed by studying two generic classes of final states:

- *Flavor specific final states.* Any final state which enables to determine unambiguously the nature (B^0 or $\overline{B}^0$) of its mother meson is called flavour specific. The simplest examples are the semileptonic decays, for which the rule $\Delta B = \Delta Q$ insures that the lepton charge gives the signature of the flavor of the B. Assuming that the flavor is known at $t = 0$, there exist two possibilities:

  - the final state f can only be produced by the flavor of the initial B. This requires the observation of a difference between the decay rates of matter and antimatter, i.e. $\Gamma(i \to f) \neq \Gamma(\bar{i} \to \bar{f})$. The interaction responsible of the desintegration of the B meson is at

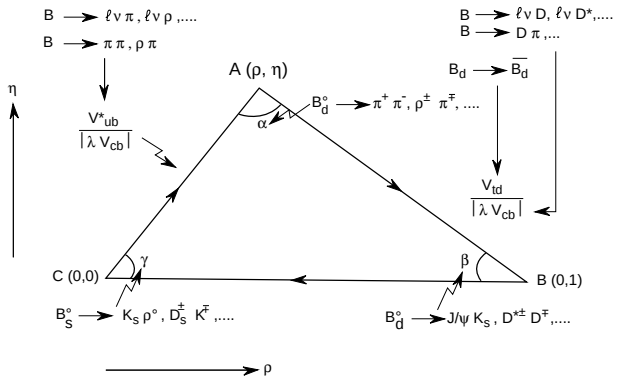

Figure 1. The unitarity triangle. Some B decay modes which allow to measure the sides and the angles are also shown.

the origin of CP violation. This is called **Direct CP Violation**. Note that both neutral and charged mesons could be used.

In general, decay amplitudes can be factorized into its magnitude and their weak and strong phases, $\mathcal{A} = \mid \mathcal{A} \mid e^{i\phi_W} e^{i\phi_S}$. Under CP transformation only the weak phases are modified, $\overline{\mathcal{A}} = \mid \overline{\mathcal{A}} \mid e^{-i\phi_W} e^{i\phi_S}$. As decay rates are proportional to the total amplitude squared, processes involving at least two decay amplitudes may result into CP violating effects. The following conditions have to be satisfied: i) the magnitudes of the amplitudes should be of the same order; ii) the amplitudes must have different weak and strong phases. The expected asymmetries might be large (with large uncertainties) but the branching ratios of the interesting modes are small ($\sim 10^{-5}$). About $10^9 - 10^{10}$ B mesons could be necessary to be sensitive to any asymmetry. In addition, these asymmetries are hard to interpret in terms of the angles of the Unitarity Triangle, given the difficulty to estimate with reasonable confidence the amplitudes and the strong phases (mainly due to the presence of penguin diagrams). An exhaustive list of potential modes can be found in [15]. The interpretation of CP violating effects in terms of the angles of the Unitarity Triangle may be better achieved by studying the decays $B^{\pm} \to D^0(\bar{D}^0)K^{(*)\pm}$ and $B^0 \to D^0(\bar{D}^0)K^{*0}$, $K^{*0} \to K^+\pi^+$ [15,16], which would allow to measure γ.

– the final state f cannot be produced by the flavour of the initial B.

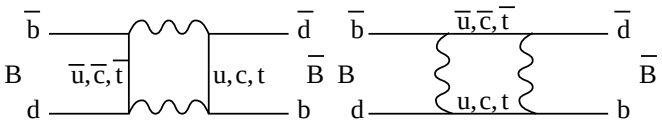

Figure 2. Feynman diagrams responsible for the $B^0\overline{B}^0$mixing

This is equivalent to impose $B^0\overline{B}^0$ mixing. In the SM, $B^0\overline{B}^0$ mixing is induced by box diagrams involving the top quark, as shown in Fig. 2. The time dependence for a B^0 state can be written as
The time dependence for a B^0 state is

$$\begin{aligned} \mid B^0(t)\rangle = \tfrac{1}{2}e^{-i(m-i\Gamma)t}[\cos(\Delta m_d t/2) \mid B^0\rangle \\ + i\sin(\Delta m_d t/2) \mid p/q \mid e^{2i\phi_M} \mid \bar{B}^0\rangle] \end{aligned} \tag{6}$$

where $\phi_M = \arg(V_{td}V_{tb}^*)$ is the mixing phase. m and Γ are the mean mass and width values of the two mass eigenstates. A similar expression for the evolution of a $\overline{B}^0$ meson is obtained by changing B^0 by $\overline{B}^0$ (and vice versa) and changing the sign of the mixing phase. In the context of the SM, $\mid p/q \mid \approx 1$.
In this case one may search for the asymmetry

$$\mathcal{A}_s(t) = \frac{\Gamma(\bar{B}^0(t) \to f) - \Gamma(B^0(t) \to \bar{f})}{\Gamma(\bar{B}^0(t) \to f) + \Gamma(B^0(t) \to \bar{f})} \tag{7}$$

This asymmetry is solely due to $B^0\overline{B}^0$ mixing, revealing that $B^0 \to \overline{B}^0$ is not equivalent to $\overline{B}^0 \to B^0$, and therefore is a measurement of T violation. This is called **CP Violation in Mixing**. If $B^0\overline{B}^0$ pairs are produced, this asymmetry can be observed, for example, by studying the difference between the number of same sign positive leptons ($\ell^+\ell^+$) and same sign negative leptons ($\ell^-\ell^-$). The expected asymmetries are, however, small, $\mathcal{A}_s < 2 \times 10^{-3}$, and about 10^{10} B mesons are required in order to measure any asymmetry, what makes this measurement very difficult to observe, requiring an excellent understanding of systematic effects. However, it is very important to make this measurement since any sizeable asymmetry (say larger than 1%) would be a clear indication of New Physics.

- *Non-flavor specific final states.* All final states reachable by both B^0 and $\overline{B}^0$ belong to this class, and the condition is fulfilled by any state which

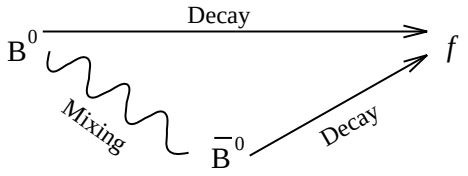

Figure 3. Interplay between direct decay and mixing in CP violation.

is a CP eigenstate, $CP \mid f_{CP}\rangle = \eta_{CP} \mid f_{CP}\rangle$, where η_{CP} is the CP parity of the final state ($\eta_{CP} = \pm 1$). Therefore in this case there will be an interference between direct decay and $B^0\overline{B}^0$ mixing, as shown in Fig. 3.

The time-dependent asymmetry (7), now to a CP eigenstate ($f \to f_{CP}$), reads

$$\mathcal{A}_s(t) = \eta_{CP} \sin 2(\phi_M + \phi_D) \sin \Delta m_d t \tag{8}$$

where ϕ_D is the decay phase coming from the desintegration process. Equation (8) assumes that direct CP violation does not occur, otherwise a more complicated expression would be derived. This situation is called **CP Violation from the interplay between decay and mixing**.

This is the most promising source of measurable CP violation and it is expected to be the major result of the Asymmetric B Factories. Color-suppressed modes ($b \to c\bar{c}s$, see Fig. 4), like $B^0 \to$ Charmonium $+K^0_S(K^0_L)$ and the corresponding modes with K^*, where the K^* decays into a CP eigenstate, $K^* \to K^0_S\pi^0(K^0_L\pi^0)$ are, from both the theoretical and experimental point of views, the suitable modes for that purpose. For these modes $\phi_D = \arg(V_{cs}V^*_{cb}) \approx 0$ and $\phi_M = \beta$, with negligible theoretical uncertainty [15]. They have reasonable branching ratios and in principle, controllable backgrounds (specially the so-called "gold-plated" mode, $B^0 \to J/\Psi K^0_S$). A summary of some of the most promising final states which can be used for observing time-dependent CP violation asymmetries can be found in table 1 (taken from [15]).

2 Experimental Considerations

The primary goal of the Physics program at the Asymmetric B Factories will be the systematic study of CP asymmetries in the B^0 decays, providing redundant measurements of the sides and angles of the Unitarity Triangle. The

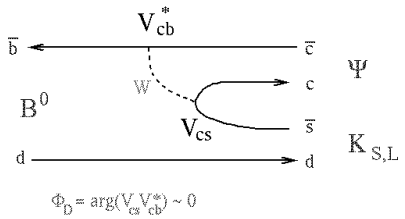

Figure 4. Feynman diagrams responsible for the color suppressed CP modes, $B^0 \to J/\Psi K_S^0$ and $B^0 \to J/\Psi K_L^0$.

Table 1. Examples of some promising $B^0(\overline{B}^0)$ decays which can be used for observing time-dependent CP violation asymmetries. V and P denotes, respectively, Vector and Pseudoscalar.

Modes	Class 1 (V-P)	Class 2 (P-P)	Class 3 (V-V)	Measured angle	Penguin contribution
$b \to c\bar{c}s$	$J/\psi K_S^0$, $J/\psi K_L^0$ $\psi(2S)K_S^0$, $\psi(2S)K_L^0$ $\chi_{c1}K_S^0$		$J/\psi K^{*0}$ $(K_S^0\pi^0)$	$\sin 2\beta$	negligible
$b \to c\bar{c}d$	$D^{*+}D^-$	D^+D^- $D^0\bar{D}^0$	$D^{*+}D^{*-}$	$\sin 2\beta$	small
$b \to u\bar{u}d$	$\rho^+\pi^-$ $\rho^0\pi^0$, $a_1^+\pi^-$	$\pi^+\pi^-$	$\rho^+\rho^-$	$\sin 2\alpha$	possible ($< 20\%$)

measurement of time-dependent CP violating asymmetries (due to interplay of decay and mixing) plays one of the central roles and it imposes stringent conditions on both, the machines and the detectors. It requires the reconstruction of exclusive final states which can be produced in B^0 and $\overline{B}^0$ decays. In general, the branching ratios of such modes are small ($10^{-4} - 10^{-5}$), therefore it is necessary the production of large amounts of B^0 mesons ($\sim 10^8$) as well as to have a very large trigger and reconstruction efficiencies, including final states with π^0's and γ's, keeping backgrounds low.

The number of produced B^0 mesons depends on the $b\bar{b}$ cross-section and the luminosity. However, one needs to consider also the cleanliness of the environment in which the B mesons are produced. In other words, what are the reconstruction and tagging efficiencies and what is the signal over

background ratio? One of the most appropriate choices seems to be a "factory mode" of the e^+e^- colliders at the $\Upsilon(4S)$ energy (10.6 GeV). There are many advantages in this choice:

- although not huge, the $b\bar{b}$ cross-section is acceptable, $\sigma(e^+e^- \to \Upsilon(4S) \to b\bar{b}) \approx 1.05$ nb;
- the $\Upsilon(4S)$ resonance ($J^{PC} = 1^{--}$) decays into a pair of $B\overline{B}$ mesons, $\sim 50\%$ B^+B^-, $\sim 50\%$ $B^0\overline{B}^0$;
- it is the cleanest source of $B\overline{B}$ pairs:
  - no other particle is produced, allowing to get a good tagging efficiency (see later);
  - event multiplicity is small, ~ 10 charged tracks and ~ 10 photons are produced in average, and the tracks/clusters are spread over the full solid angle. Therefore the reconstruction efficiency is large (included π^0's and γ's) with rather small background contribution, mainly due to continuum events;
  - off-resonance peak running (about 40 MeV below the peak) allows background subtraction using data;
- stringent kinematic constraints can be applied. For instance, the measurement of the B mass can be improved in about one order of magnitude by using the energy of the beam as energy of the B;
- coherent $B\overline{B}$ production. Since the $\Upsilon(4S)$ decays exclusively into a $B\overline{B}$ pair, the $B\overline{B}$ system is in a coherent (antisymmetric) quantum state,

$$\frac{|\, B(t_1)\overline{B}(t_2)\rangle - |\, \overline{B}(t_1)B(t_2)\rangle}{\sqrt{2}} \tag{9}$$

  and must be considered as a whole instead of the individual B mesons. The system will evolve coherently until one of them decays. It is only at that time (reference time, t_0) that the nature of the second meson (B^0 or $\overline{B}^0$) will be defined: the flavor of the second B^0 will be opposite to that of the first B^0 and the time of the second B^0 (t_1) can be measured relative to the first one, $\Delta t = t_1 - t_0$. This is the well known EPR paradox [17], applied to the $\Upsilon(4S)$ system (illustrated in Fig. 5).

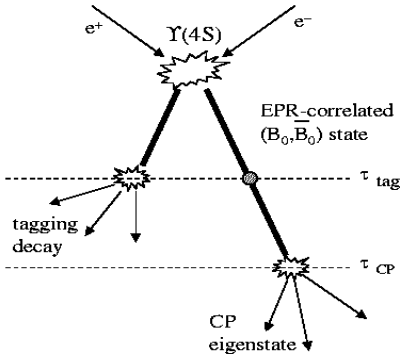

Figure 5. EPR paradox in the $\Upsilon(4S)$ system: even though both B^0's mix, when we measure (tag) the flavor of one of the B^0's, then it is defined the flavor of the other which has to be its CP conjugate at that time. Then we can measure the decay time of the other B^0 relative to the time that the first one was tagged.

The main limitation is coming from the achievable luminosity of the collider. In this area there is a clear advantage for the hadronic collisions [18]. Integrated luminosities between 30 and 100 fb^{-1}/year and several years of operation will be required. This will be achieved only with peak luminosities larger than 10^{33} $\text{cm}^{-2}\text{s}^{-1}$.

The measurement of time-dependent CP violating asymmetries (due to interplay of decay and mixing) imposes also an additional, serious constraint to the $\Upsilon(4S)$ experiments. The reference time, t_0, is not the $\Upsilon(4S)$ decay, but the time at which one of the B's is identified. The consequence is that since the terms with $\sin \Delta m_d \Delta t$ can have positive and negative values, the $\sin \Delta m_d \Delta t$ term vanishes when integrating over time, i.e. no CP violating effect involving interplay between decay and mixing can be observed. It is therefore mandatory to measure Δt, which can be extracted by measuring the relative flight distance of the B mesons, $\Delta L = \beta\gamma c \Delta t$, where β is the B meson velocity. However, at the $\Upsilon(4S)$ energy, B mesons are produced almost at rest ($p_B \approx 300$ MeV/c) in center-of-mass frame and the average distance between both B decay vertices is only about 50 μm, which is of the same order than the resolution achievable with present technologies, making difficult to measure any time-dependent mixing. However, if the collider is asymmetric, then the system is Lorentz boosted along the direction of the high energy beam and then the time measurement can be performed through

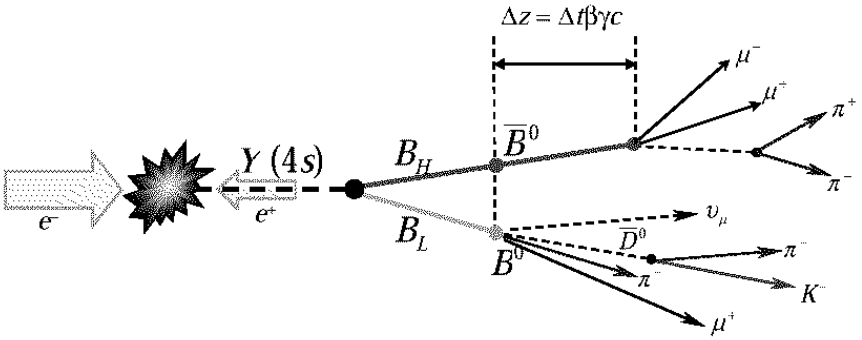

Figure 6. A schematic view of the event topology at Asymmetric B Factories.

a Δz position measurement. These asymmetric energies give rise to the event topology sketched in Fig. 6.

The distance Δz can be written in terms of t_0 and t_1,

$$\Delta z = \beta\gamma c\tau \frac{t_1 - t_0}{\tau} + \gamma\beta_{CM} c\tau \cos\theta_B^* \frac{t_1 + t_0}{\tau} \ . \tag{10}$$

In this equation, $\beta\gamma$ is the boost of the $\Upsilon(4S)$, $c\tau$ is the average flight distance of a B meson and β_{CM} is its velocity in the $\Upsilon(4S)$ frame ($\beta_{CM} \approx 0.07$). θ_B^* is the angle at which the B meson is produced in the $\Upsilon(4S)$ rest frame with respect to the beam direction. For most studies, the second term in (10) can be safely neglected. The minimal value of the boost $\beta\gamma$ obviously depends on the experimental resolution on Δz. Assuming $\sigma(\Delta z) \approx 110$ μm, it is suitable a mean $\Delta z = \beta\gamma c\tau$ value of ≈ 250 μm, which requires a boost of $\beta\gamma \approx 0.56$. All studies have shown that the CP asymmetry can safely be observed with the high energy beam in the range between 8 and 9 GeV[19].

3 The machines: PEP-II at SLAC and KEK-B at KEK

Many proposed feasibility studies of such a machine were carried out in several laboratories. Only two of them have been constructed at Stanford Linear Accelator Center (SLAC) in California (USA) and at KEK in Japan. These colliders (PEP-II at SLAC and KEK-B at KEK) have two rings (2.2 Km and 3.0 Km circumference, respectively) with collision at a single point (see

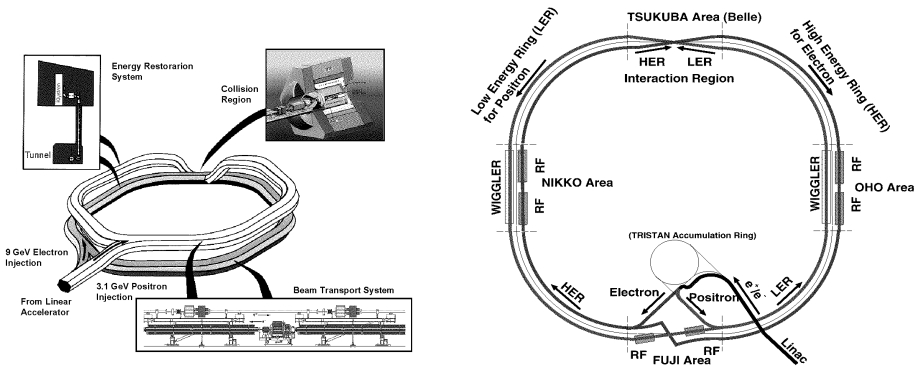

Figure 7. Sketch of the main rings of the PEP-II (left) and KEK-B (right) B Factories.

Fig. 7). The high luminosity is achiveved through high currents and strong focusing.

Both machines had a very remarkable success in all the different stages of the project, in spite of the very agressive schedules, being always on or ahead schedule. Tables 2 and 3 summarize some of the most relevant design and achieved performances of these two machines. As as reference, here a some of the milestones of the PEP-II project:

- May '97: starts commissioning of the HER (High Energy Ring);
- July '98: LER (Low Energy Ring) installation completed. HER running with 1222 bunches and with a current 759 mA/bunch;
- February '99: LER current 1171 mA (world record);
- March '99: commissioning was put on hold to install the detector (*BABAR*). By this point, PEP-II has already achieved a luminosity of 5.2×10^{32} cm^{-2}s^{-1} with 786 bunches.
- May '99: First collisions recorded with *BABAR*. PEP-II achieved the world record luminosity of 1.4×10^{34} cm^{-2}s^{-1}. Fig. 8 shows the integrated and daily luminosity history of PEP-II and the *BABAR* experiment. The inactive period near October '99 was a planned shutdown to install some remainder components of the detector. There was an inactive period starting in November '99 until the end of the year due to a PEP-II vacuum leak. Finally, PEP-II delivered 2 fb^{-1}on-resonance data, of wich 1.7 fb^{-1}were recorded by *BABAR*.

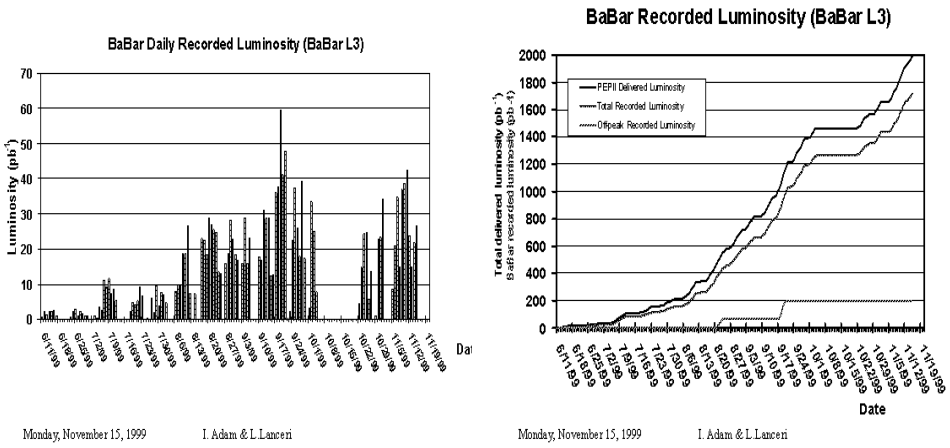

Figure 8. Daily (left) and integrated (right) luminosity history of PEP-II and the *BABAR* experiment.

Apart from the luminosity, the main difficulty of B Factories is to keep the background accelerator at a level manageable by the detectors and physics. The "acceptable" level of background is determined primarily by the radiation hardness of silicon detectors and electromagnetic calorimeters, and by requiring a tolerable drift chamber currents. The trigger rate, the occupancy of other subdetectors, the stress of the pattern recognition algorithms and the saturation of storage capacities can also constitute occasional limitations. Therefore, it is mandatory a careful monitoring, analysis and simulation of the background sources and their impact. Only in this way effective remediation of their effects can be found to insure the safety, data quality and the useful lifetime of the experiment.

The primary causes of accelerator-induced backgrounds are:

- synchroton radiation generated in the bending magnets and final focusing quadrupoles in the incoming HER and LER beam lines. These magnets also impose strong mechanical constraints to the detector. As an example, in *BABAR* permanent magnets reach into the region $\mid z \mid = 21$ cm [20].

- two-beam backgrounds from three sources: enhanced beam-gas interac-

Table 2. Design and achived performances (December 1999) of the PEP-II Asymmetric B Factory at SLAC..

Parameter (design/achieved)	HER e^-		LER e^+
Beam Energy (GeV)	9.0/9.0		3.1/3.1
Boost ($\beta\gamma$)		0.56	
Current/bunch (mA)	0.6/0.6		1.3/1.3
# bunches	1658/829		1658/829
Total current (A)	0.75/0.55		2.1/1.7
Bunch spacing (m)		1.26	
σ_z (cm)	1.0		1.15
σ_x at IP (μm)		220/200	
σ_y at IP (μm)		6.6/6.3	
Lifetime	4h@1A/ 8h@0.5A		4h@2A/ 2.7h@0.8A
1/2 crossing angle (mrad)		0 (head-on)	
Peak luminosity ($\mathrm{cm}^{-2}\mathrm{s}^{-1}$)		$3 \times 10^{33}/1.4 \times 10^{33}$	
Recorded luminosity		2 fb^{-1}	

Table 3. Design and achived performances (December 1999) of the KEK-B Asymmetric B Factory at KEK..

Parameter (design/achieved)	HER e^-		LER e^+
Beam Energy (GeV)	8.0/8.5		3.5/4.0
Boost ($\beta\gamma$)		0.425	
Current/bunch (mA)	0.22/4		0.52/2.3
# bunches	5000/800		5000/1024
Total current (A)	1.10/0.51		2.6/0.53
σ_z (cm)	0.40/0.56		0.40/0.56
σ_x at IP (μm)		77/170	
σ_y at IP (μm)		1.9/2	
Lifetime	4.2h@0.27A		1.7h@0.43A
1/2 crossing angle (mr)		11	
Peak luminosity ($\mathrm{cm}^{-2}\mathrm{s}^{-1}$)		$1 \times 10^{34}/5.9 \times 10^{32}$	
Recorded luminosity		300 pb^{-1}	

tions due to low-energy interaction point synchroton radiation impinging onto the incoming beam pipe; photons and low energy $e^{\pm}$ from radiative Bhabha scatering hitting nearby vacuum components; tails generated by

the beam-beam interaction and/or by the electron-cloud-induced blowup of the low energy beam.

- the interaction of beam particles with residual gas around the rings (beam-gas), which constitutes the primary source of radiation damage, and that with the largest impact on operational efficiency.
- optics mis-tuning and injection losses.

Reduction of these sources involve a strict program of local lead shielding, masking, collimators, vacuum pumping, real-time radiation monitoring and beam dump hardware interlock systems.

4 The detectors: *The Beauty* and *The Beast*

Based on the physics motivations of section 1 and the experimental considerations described in section 2, the general requirements of the detectors are:

- exclusive B meson reconstruction of low branching ratio modes, with potentially high backgrounds (accelerator-induced and physics) demand:
  - excellent momentum ($\sim 0.5\%$) and energy resolution;
  - good acceptance in forward direction;
  - track reconstruction down to 50 MeV/c in transverse momentum;
  - pion/kaon separation up to 4 GeV/c (this is required to separate $B \to \pi\pi,\ K\pi,\ KK$ decays);
  - detection of π^0's and γ's (20 MeV/c^2-5 GeV/c^2);
  - lepton identification;
  - K_L^0 detection capability;
- B flavor tagging heavily relies on lepton and kaon identification:
  - lepton identification down to 500 MeV/c;
  - kaon identification below 2 GeV/c;
- a resolution on Δz about 110 μm is needed, therefore high precision vertexing should be possible. Given the low momentum range of the tracks, errors will be dominated by multiple scattering. It is therefore necessary to minimize the amount of material in front of the first detector layer.

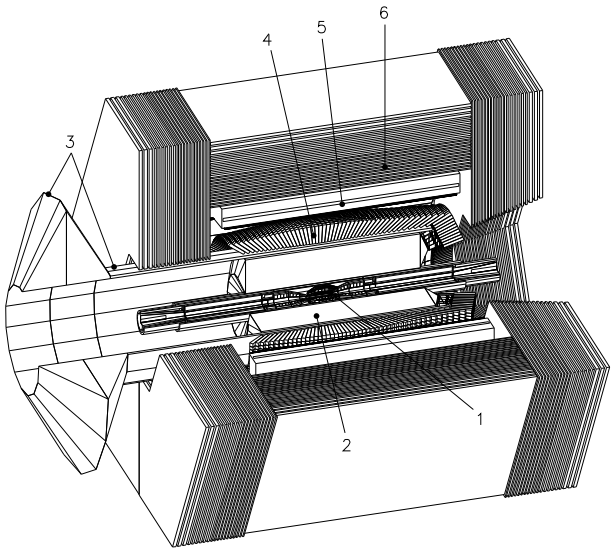

Figure 9. The *BABAR* Detector at the SLAC B Factory: 1.Silicon Vertex Tracker, 2.Drift Chamber, 3.Particle Identification Subsystem (DIRC - Detector of Internally Reflected Cherenkov Light), 4.Electromagnetic Calorimeter, 5.Magnet, 6.Instrumented Flux Return.

With these requirements, the design of the B Factory detectors, *BABAR*[20] at PEP-II and *BELLE*[21] at KEK-B, used quite conventional techniques, already in operation in other (older) facilities. They use a silicon vertex detector, a tracker which can be made of silicon detector and/or drift chambers, a particle identification system based on dE/dx, time-of-flight or Cherenkov counters or imaging devices and electromagnetic calorimetry using crystals. Fig. 9 and 10 show a schematic view of the *BABAR* and *BELLE* detector components. Table 4 give a snapshot of the different components. As it can be seen, both detectors are very similar in the chosen technologies. The most remarkable difference concerns the particle identification system.

The vertex detector information dominates the measurement of the track direction and impact parameters, both along and perpendicular to the beam direction. The *BABAR* Silicon Vertex Tracker (SVT) consists of five layers of two-sided silicon strip detectors, meanwhile the *BELLE* Silicon Vertex Device (SVD) has only three layers. Both detectors use radiation-hard technologies. The smaller size of the *BELLE* SVD detector is compensated with a larger Central Drift Chamber (CDC), with internal and external radius of 8 and 87

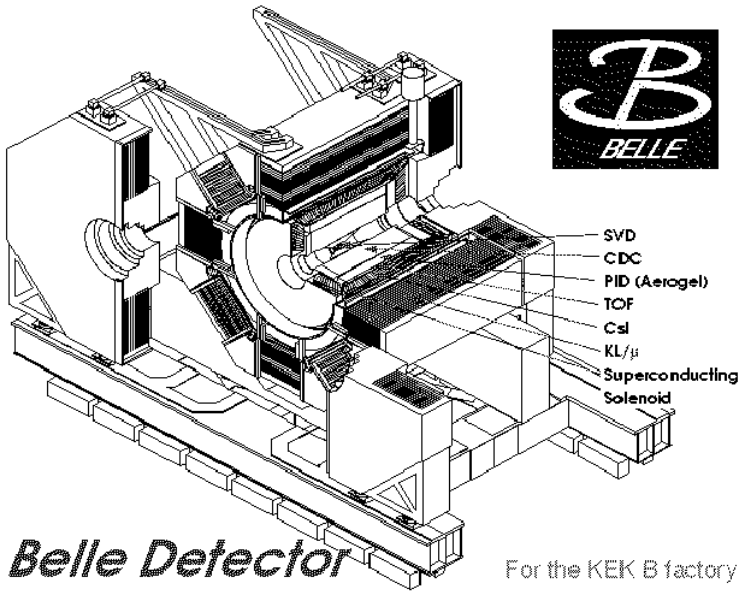

Figure 10. Schematic view of the *BELLE* Detector at the KEK-B B Factory. The different subsystems are also indicated.

cm respectively, and 50 layers. The *BABAR* Drift CHamber (DCH) contains 40 layers, and extends from 22.5 to 80 cm. Proper alignment data for all silicon wafers as well as the relative alignment between silicon and drift chamber are crucial inputs to achive the required vertex resolution. Silicon detectors constitute the main tracking system for low momentum tracks ($p_\perp < 100$ MeV/c), as it is the case of low-momentum pions from $D^{*+} \to D^0\pi^+$ decays. The spatial resolution achieved so far in the *BABAR* SVT innermost layer, as determined from the first months of data, is shown in Fig. 11 (left). It is close to the expectation from Monte Carlo simulation. Fig. 11 (right) shows the accumulated dose in the *BABAR* SVT: it can be seen that it has been maintained well below budget. Less chance had the *BELLE* SVD detector which had to be replaced by a new one after a few weeks of operation. The drift chambers provide the resolution for the measurement of the momentum of the tracks. The pulse height information provided by the drift chambers are also used to measure the mean ionization loss (dE/dx).

Table 4. Summary table of the *BABAR* and *BELLE* subsystems.

Subsystem	*BABAR*	*BELLE*
Silicon Detector	**SVT** 5 double sided radiation hard layers	**SVD** 3 double sided layers
Drift chamber	**DCH** 22.5-80 cm, 40 layers (axial/stereo)	**CDC** 8-87 cm, 50 layers (18 stereo)
Particle ID	**DIRC** Detector of Internally Reflected Cherenkov light 144 quartz bars	**ToF+ACC** 4 cm-thick scintillators, 128 ϕ segmentation 960+228 silica aerogel cells
Electromagnetic calorimeter	**EMC** 5760+820 CsI(Tl) crystals in barrel and forward endcap	**CsI** 6624+1152+960 CsI(Tl) crystals 30 cm long
Superconducting coil	1.5 T	1.5 T
μ/K_L^0 detector	**IFR** 19 RPC layers, 65 cm iron in barrel, 18 RPC layers, 60 cm iron in endcaps 2 double-layer RPC inside the coil	**KLM** 14 layers RPC superlayer and 4.7 iron

The superconducting magnet coils provide a field of 1.5T inside the tracking volume. Together with the spacial resolution, this allows a momentum accuracy about 0.3% for high-momentum tracks. The full tracking system, combining silicon and drift chambers, provides very good pattern recognition capability for charged tracks, even at periods with high machine backgrounds. Fig. 12 shows the *BABAR* impact parameter resolution, in the transverse and longitudinal planes, as a function of transverse momentum as measured with multihadron events. The asymptotic value at high momentum is about 40 μm, consistent with dimuon measurement at high momentum. A good indicator of the integrated tracking performace comes from mass resolutions. For $D^0 \to K^-\pi^+$ the mass resolution measured by *BELLE* is 6.9 ± 0.6 MeV/c^2, meanwhile it is 7.9 ± 0.4 MeV/c^2 for *BABAR* without final calibrations. The $K_S^0 \to \pi^+\pi^-$ mass distribution as measured by the *BELLE* detector is shown in Fig. 13 for two different momentum intervals, 0.5 GeV/c< P < 1.5 GeV/c and $P > 1.5$ GeV/c; the mass resolutions are, respectively, 4.3 ± 0.1 MeV/c^2 and 5.4 ± 0.3 MeV/c^2. The corresponding resolution measured by *BABAR* is 5.4 ± 0.5 MeV/c^2 averaged over all momentum range.

There are two important benchmarks of performace for the particle identification system. As indicated above, one is the ability to separate $B^0 \to \pi^+\pi^-$

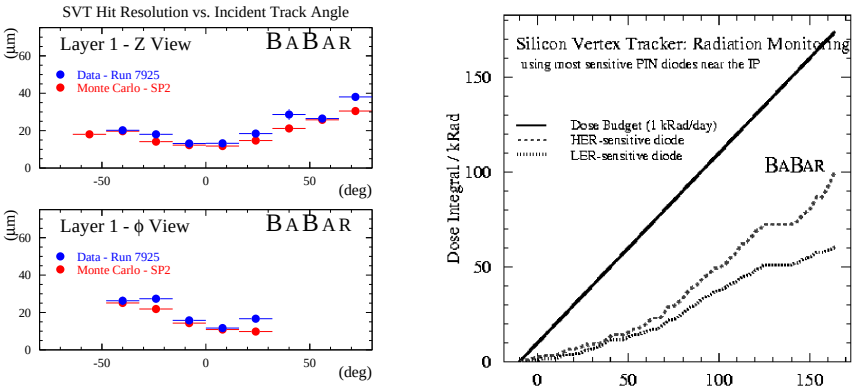

Figure 11. (Left) *BABAR* SVT point resolution as a function of the incident track angle for the innermost layer. (Right) History plot of accumulated radiation doses in the *BABAR* SVT using PIN diodes near the interaction point in the horizontal plane. The horizontal axis gives the number of days of running, and the diagonal straight line represents the alloted budget (240 kRad/year), rationing out a 100kRad dose over the detector's planned lifespan.

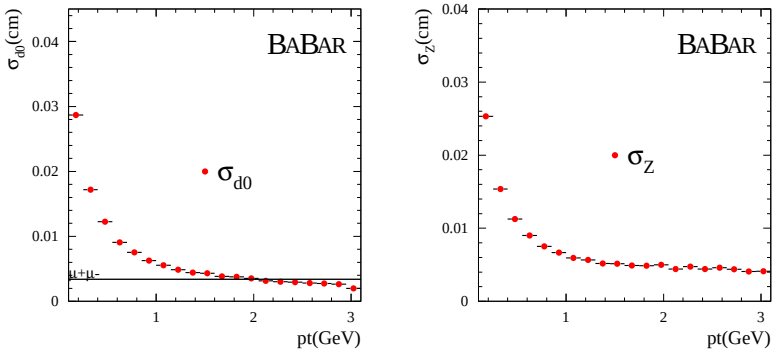

Figure 12. Impact parameter resolution as a function of transverse momentum in *BABAR*.

from $B^0 \to K^+\pi^-$ and the other is the performace of charged kaon tagging. In the case of *BABAR* this is resolved in the barrel region using a DIRC (Dectection of Internally Reflected Cherenkov light) system, a new sort of ring

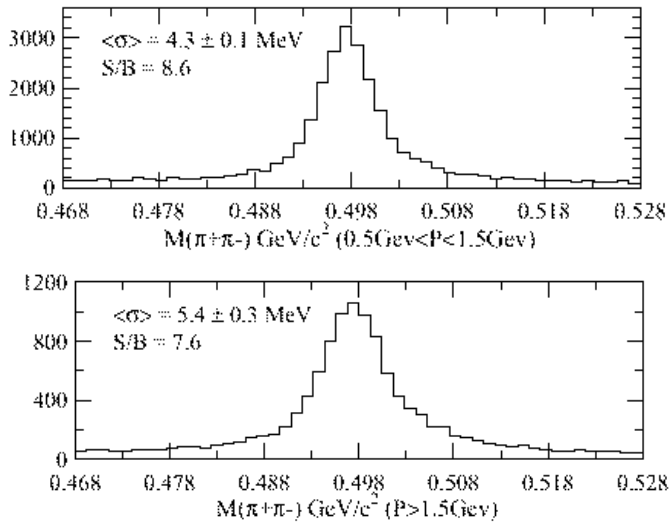

Figure 13. Mass distribution for $K^0_S \to \pi^+\pi^-$ in *BELLE* for two momentum regions: (top) 0.5 GeV/c< P < 1.5 GeV/c, and (bottom) P > 1.5 GeV/c.

imaging Cherenkov detector. This constitutes one of the main differences with respect to *BELLE* where the problem is resolved with more conventional techniques by combining a time-of-flight system and threshold aerogel counters. The *BABAR* DIRC radiator consists of 156 quartz bars of 4.7m length arranged in a 12-sided polygon around the drift chamber. As shown in Fig. 14, a charged track traversing the thin quartz bars produces Cherenkov light which is emitted at Cherenkov angle with respect to the particle direction. Part of this light hits the bar walls beyond the angle of total reflection, and is multiply reflected, until it reaches the back end, where it is transmitted via the standoff box –a purified water-filled tank– to an array of 10572 PMTs. The directions of the reflected part of the Cherenkov cone form two conic sections in the detector plane, which define the Cherenkov angle and thereby the velocity of the charged particle. The most important challenge of this detector is that the surface polish of the quartz bars has to be within 5-10 angstroms RMS. This caused about one year delay in the completion of the detector: the detector was finally completed during the shutdown in mid-October. A resolution on the Cherenkov angle, θ_C, of about 2 mrad is required for π/K

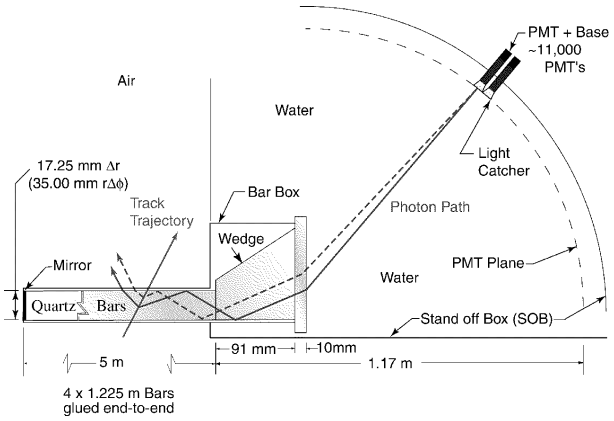

Figure 14. Schematic view of the DIRC principle of operation.

separation in the above mentioned modes. With the current data the measured resolution is 3.0 mrad. The goal for the coming months will be to reach the required resolution. Very significant improvements which will allow to reach the design resolution are expected with better alignments, calibrations and tuning of the detector.

The photon energy region of interest for B physics ranges from about 20 MeV to 4 GeV in laboratory frame. The B mass resolution for modes such as $\pi^0\pi^0$ or $\rho\pi$ is dominated by the photon energy resolution. The optimum calorimeter design to achieve good resolution over this wide range is a structure of Tl-doped CsI crystals. *BABAR* and *BELLE* both use this technology for their electromagnetic calorimeter. These subsystems are also used for electron identification. Fig. 15 shows the invariant mass of all combinations of neutral clusters (photon candidates) for *BABAR* and *BELLE* data. The measured π^0 mass resolutions are, respectively, 6.9 MeV/c^2 and 5.4 MeV/c^2.

Outside the magnet there are finally the μ/K_L^0 subsystems which primary goal is to reduce the lower momentum limit for cleanly identify muons. This increases the efficiency for tagging the flavor of B mesons substantially, and it also increases the size of the lepton sample for studies of semileptonic decays. The iron gaps of these detectors are instrumented with resistive plate chambers (RPC). In addition to its primary goal to identify muons, these systems can identify K_L^0 mesons to measure their angle with good precision to detect $B^0 \to J/\psi K_L^0$ decays.

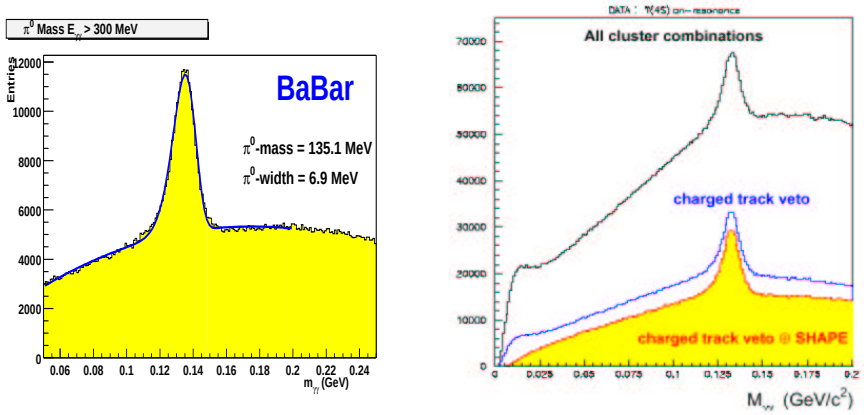

Figure 15. Reconstructed $\pi^0 \to \gamma\gamma$ mass for (left) *BABAR* and (right) *BELLE*. *BABAR* (*BABAR*) selection requires a minimum γ energy of 100 MeV (50) and a minium π^0 energy of 500 MeV (500).

Table 5 compares some of the most relevant performace parameters for *BABAR* and *BELLE*. It can be seen that they have similar performances, which is certainly not surprising given that they use similar technologies. It can be safely anticipated that important improvements are expected in the coming months thans to a better detector understanding which will reflect in better calibrations, alignments and agreement between data and Monte Carlo simulations. The coming improvements in the reconstruction software will significantly contribute.

5 Preparation for CP Physics

The analysis of the collected data by *BABAR* and *BELLE* is still in an early stage. After the first collisions, most of the activity has been centered in tuning-up the accelerators, detectors, reconstruction and physics tools.

One of the first results from the experiments has been the cross-section determination. The ratio between the number of multihadron events and Bhabha events, $r = N_{hadronic}/N_{Bhabha}$, as a function of the center-of-mass energy, is shown in Fig. 16 using *BABAR* data. The peak position is used during these first stages of the experiments to set the absolute scale of the accelerator, requiring the fitted mass to be 10.580 GeV.

Table 5. Summary of the *BABAR* and *BELLE* detector performaces..

BABAR	*BELLE*
σ_{hit}(DCH)=125 μm average for Bhabha (exceeds specifications of 140 μm)	σ_{hit}(CDC)=149 μm average for Bhabha
$\sigma(dE/dx)$ = 7% for Bhabha	$\sigma(dE/dx)$ = 9% for pions, 7% for Bhabha
$\sigma(\theta_C)$ = 3.0 mrad for Bhabha (2.0 mrad specifications)	σ(ToF)=100 ps for dimuons
σ_z(SVT)=19 μm for cosmics	σ_z(SVT)=45 μm for cosmics above $p \sin\theta^{5/2}$=2 GeV/c
$\sigma_E/E = 1\%E(\text{ GeV})^{-1/4} + 1.2\%$ at $\theta = 90^o$	$\sigma_E/E = 2\%$ for $e^+e^- \to \gamma\gamma$
$dp_\perp/p_\perp = 0.30\% \times p_\perp$ for $p_\perp > 1$ GeV/c	$dp_\perp/p_\perp = 0.25\% \times p_\perp + 0.39\%$
$\sigma(\pi^0) \approx 5.7\%$	$\sigma(\pi^0) \approx 4\%$
$\sigma(m_{K^0_S}) \approx 1.0\%$	$\sigma(m_{K^0_S}) \approx 0.9\%$
$\sigma(m_{D^0}) \approx 0.4\%$	$\sigma(m_{D^0}) \approx 0.4\%$

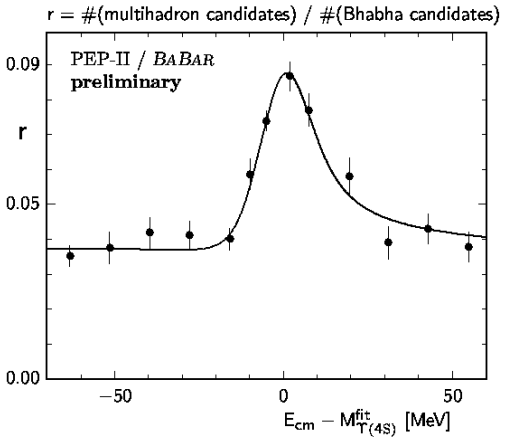

Figure 16. The ratio of multihadron to Bhabha candidates selected from samples recorded at different center-of-mass energies in *BABAR*. The curve shows the best fit to the data. The multihadron selection enhances the contribution of $\Upsilon(4S)$ decays over continuum hadronic events. A similar distribution with similar precision has been obtained by the *BELLE* experiment.

The preparation for CP violation studies is now focusing on the "golden-plated" mode, $B^0 \to J/\Psi K^0_S$. Besides the theoretical cleanliness of this mode, it has many experimental advantages: i) it has a clean signature with very low background, ii) it has low multiplicity with no neutrals (although the

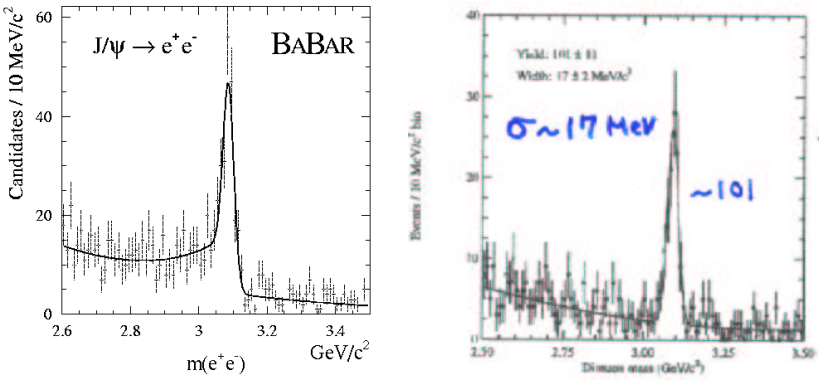

Figure 17. Mass distribution for $J/\psi \to e^+e^-$ in *BABAR* (left) and $J/\psi \to \mu^+\mu^-$ in *BELLE* (right). The low mass tail in the case of $J/\psi \to e^+e^-$ is due to bremsstrahlung.

$K^0_S \to \pi^0\pi^0$ could be also used) so it has a good reconstruction efficiency; iii) is has a relatively large rate, $BR \approx 3.7 \times 10^{-5}$. As it has been already described in previous sections, three essential ingredients are necessary to display a time dependent asymmetry:

- reconstruction of the final state;
- identify the flavor of the B meson at $t = 0$;
- measuring its decay time from its decay flight length.

J/ψ candidates are formed by combining e^+e^- and $\mu^+\mu^-$ pairs coming from a common vertex. Electrons are identified requiring shower shape to be consistent with expectations and the ratio of energy measured in the calorimeter to the measured track momentum close to unity. Muons are identified by requiring minimum ionizing tracks within the calorimeter and hits in the μ/K^0_L detectors. The mass distributions for e^+e^- and $\mu^+\mu^-$ as obtained by *BABAR* and *BELLE* respectively are shown in Fig. 17. The resolution for both cases is about 16 MeV/c^2. Significant improvements are expected from better alignments and from the use of bremsstrahlung recovery algorithms (in the case of the e^+e^- channel).

$B^0 \to J/\Psi K^0_S$ decays are found by selecting events with a J/Ψ candidate and combining it with a K^0_S candidate which form a B^0 with the expected

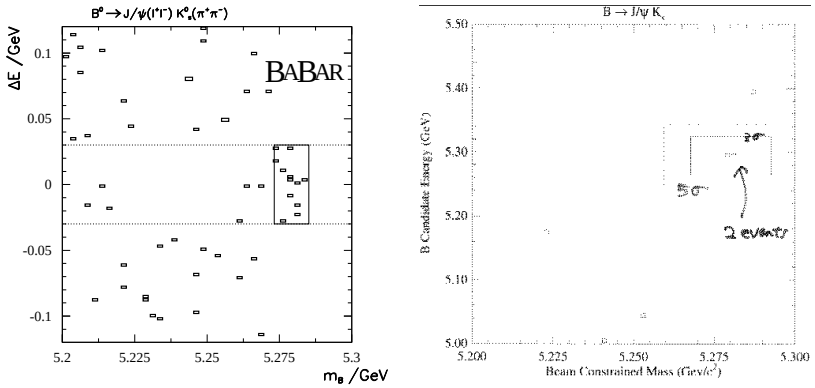

Figure 18. ΔE vs m_B distributions for the $B^0 \to J/\Psi K^0_S$ decay mode from 620 pb^{-1} of *BABAR* data (left) and 125 pb^{-1} of *BELLE* data.

mass. Mass constrained J/Ψ and K^0_S candidates are constrained to come from the same vertex. Two selection variables are used:

- $\Delta E = E^{cm}_B - E^{cm}_{beam}$, the difference between the energy of the reconstructed B meson and the beam energy in the center-of-mass frame;
- $m_B = \sqrt{(E^{cm}_{beam})^2 - (p^{cm}_B)^2}$, the mass of the B meson calculated using the beam energy and the momentum of the B. This variable, known as beam-energy substituted mass, improves in about one order of magnitude the B mass resolution.

Fig. 18 shows the distribution of events in the $\Delta E - m_B$ plane for *BABAR* and *BELLE*. From about 620 pb^{-1} *BABAR* observes a total of 12 events in the signal box, with an estimated background of 1.4. With 125 pb^{-1}, *BELLE* has 2 candidates. In both cases yields agree with expectations.

A similar analysis can be performed using $B^+ \to J/\Psi K^+$ decays. This decay mode provides an important control sample since it is very similar to $B^0 \to J/\Psi K^0_S$, but it is much more abundant ($BR \approx 1.2 \times 10^{-4}$) and with no expected CP asymmetry. The equivalent two dimensional distributions for this mode are shown in Fig. 19. In this case, *BABAR* has 32 candidates with 4.9 expected background, meanwhile *BELLE* observes 7 events. Again, yields agree with expectations.

Tagging the initial flavor of a B meson can be performed exploiting the correlation between the flavor and the charge of the decay products. Tagging

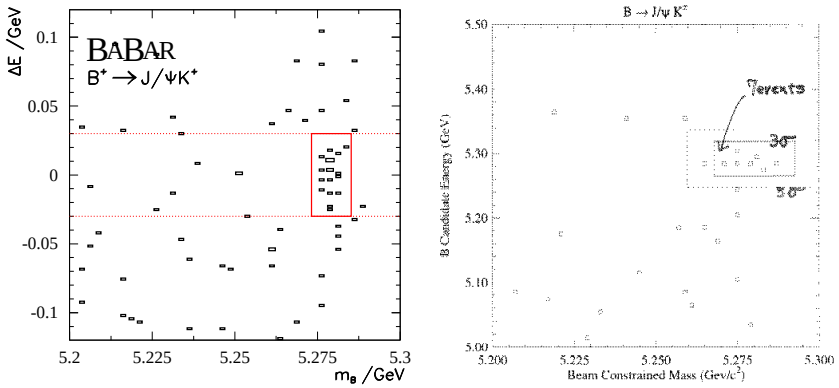

Figure 19. ΔE vs m_B distributions for the $B^0 \to J/\Psi K^0_S$ decay mode from 620 pb^{-1} of *BABAR* data (left) and 125 pb^{-1} of *BELLE* data.

mainly relies on leptons and kaons. However, some additional information can still be extracted from other decay products, such as soft leptons from charm semileptonic decays and soft pions from D^* decays. The use of multivariate methods such Neural Networks can help when combining all the information. The effective flavor tagging efficiency is given by $Q = \sum_i \epsilon_i (1-2w_i)^2$ where the sum is over tagging categories, each characterized by a tagging efficiency ϵ_i and a probability to mis-identify the B flavor, w_i. Q is related to the statistical significance of the CP asymmetry measurement ($1/\sigma^2_{stat} \sim N_{B_{\rm TAG}} Q$). At Asymmetric B Factories, Q values about 35% are expected [15]. This has to be compared to values about $\sim 10\%$ at hadronic machines [18].

Leptonic tagging is based on the charge of the lepton produced from the decay $b \to l\nu c$, as can be seen from Fig. 20(left)a) and c). The semileptonic branching ratio is about 20%, therefore these decays are a good tagging tool. Backgrounds (wrong tagging) are mainly due to fake lepton identification and cascade leptons, as shown in Fig. (left)b). Cascade lepton contribution can be strongly reduced by removing low momentum leptons.

Kaon tagging is based on the direct cascade $b \to c \to s$ shown in Fig. 20(right). Here the charge of the $s(\bar{s})$ quark is the same as the charge of the $b(\bar{b})$ quark, and therefore if the s quark produces a charged kaon, its charge should have the same sign as the charge of the initial $b(\bar{b})$ quark. Unfortunately there are other sources to produce $s(\bar{s})$ quarks in B decays and some of them lead to incorrect tagging. In Fig. 20 the wrong sign s quark

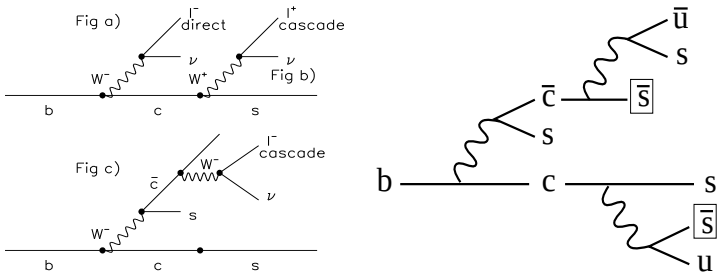

Figure 20. The different sources of production of leptons (left) and s quarks (right) from b quark decays.

has been encircled. These contributions represent about 10% to 15% of b decays. In order to identify such decays, it is useful to observe all the charged and neutral kaons in the event. This can only be effective if the detector acceptance is very good and if the particle identification is very good. *BABAR* and *BELLE* detectors have been designed to fulfill with these requirements.

Flavour specific B^0 decays, like $B^0 \to D^{*-}\pi^+$ and $B^0 \to D^{*-}\ell^+\nu$, will be used to calibrate the flavor tagging purity (mistag rate, w) to be used in the CP asymmetry measurement. Fig. 21 shows the $B^0 \to D^{*-}e^+\nu$ signal from *BABAR* (similar results has been recently reported by *BELLE*). In Fig. 21(left), the horizontal axis is the missing mass due to the neutrino, and the vertical axis is the $D^* - D^0$ mass difference. The right part of the same figure shows the projection on the vertical axis for the the missing mass signal region.

Once a B meson has been reconstructed and its initial flavor is tagged, the next step is to measure the distance Δz between the reconstructed B and the vertex of the tagging B. The main advantage of the asymmetric B Factories is that only the B mesons are produced (absence of fragmentation products) and stringent constraints can be applied from the knowledge of the IP region and $\Upsilon(4S)$ four-momentum. The main problem to overcome is the small boost of the B mesons (which will reflect in a small average decay length $\langle d \rangle$ and therefore small $\sigma_d/\langle d \rangle$) and the low energy of their decay products, therefore it is mandatory to minimize the amount of material in front of the first detector layer. The estimated Δz resolution from *BABAR* and *BELLE* is $\sim$ 110 μm, and it can be parameterized by a narrow ($\sim$ 80 μm) and a wider ($\sim$ 200 μm) Gaussian. By comparison, the vertex resolution of the fully reconstructed $B^0 \to J/\Psi K^0_S$ decay is $\sim$ 40 μm.

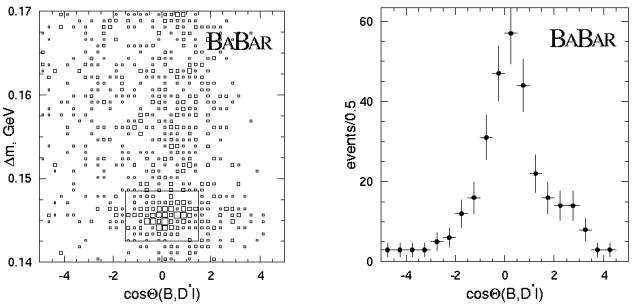

Figure 21. (Left) $D^* - D^0$ mass difference vs missing mass for $B^0 \to D^{*-} e^+ \nu$ candidates in *BABAR*. (Right) Projection on the $D^* - D^0$ mass axis for signal events in missing mass.

6 Summary and prospects

Asymmetric B Factories at SLAC (USA) and KEK (Japan) are embarked on an exciting program to study CP violation. The first physics quality data are already on tape. Accelerators are operating well and delivering colliding beams with tolerable background levels. CP Violation in the B sector will make a definite test of the Standard Model. The B meson systems are particularly suited for such studies since theoretical uncertainties in SM predictions can be well understood in some decay modes. Hadronic effects are either not present or can be measured experimentally. The "golden-plated" mode, $B^0 \to J/\psi K^0_S$ is a such decay mode. With these measurements coming, one can then overconstrain the Unitarity Triangle and, who knows, perhaps unearth the largely searched inconsistency in the Standard Model.

The performance of the detectors has been studied in the early data and found to be close, and in some cases exceeding, the design goals. Signals in the $B^0 \to J/\psi K^0_S$ and other key channels have been confirmed at the expected rates and resolutions. Studies of vertex resolution are found in reasonable agreement with simulation. The performance of the flavor tagging is being studied using flavor specific B^0 decays. By unavoidable personal bias, many of the examples provided in this talk have been based on the *BABAR* experiment. However, it has been shown the similarities in the design and early performances of *BELLE*. During the first months of data taking both experiments many problems but fortunately the hard work of engineers and physicists allowed to overcome them.

The short term goal of the *BABAR* and *BELLE* Collaborations is to accu-

mulate about 10 fb^{-1} for Summer 2000 to perform a first measurement of $\sin 2\beta$. In addition, a rich problem of other physis measurements is underway: B oscillations and B lifetimes, overall CKM contributions, direct CP violation, charm physics, τ physics and $\gamma\gamma$ physics.

This document summarizes the situation of B Factories at the time of this Conference. However, when writing these proceedings, the situation has dramatically changed, and the experiments have already presented their first results (including CP violation asymmetry) at the XXX^{th} International Conference on High Energy Physics, Osaka (Japan).

Acknowledgments

It is a pleasure to thank the organizers for the splendid organization of the Meeting, the wonderful place were it took place and also for the possibility they bring to me to give this talk. My special thanks to M. Aguilar-Benítez and J. Alcaraz by their indeed warmly invitation and Conference Dinner. And I do not forget Mercedes Fatás, by her unlimited patience and efficiency.

References

1. I.I. Bigi, A.I. Sanda, *CP Violation*, Cambridge University Press, 2000.
2. J.H. Christenson, J.W. Cronin, V.L. Fitch and R. Turlay, Phys. Rev. Lett. **13** (1964) 138.
3. A.D. Sakharov, Pis'ma Zh. Ekps. Teor. Fiz. **5** (1967) 32.
4. For a review of Cosmological Consequences of GUTs see: D.V. Nanopoulos, Prog. in Particle and Nuclear Physics **6** (1980) 23.
5. V.A. Kuzmin, V.A. Rubakov and M.E. Shaposhnikov, Phys. Lett. B **155** (1985) 36.
6. M.E. Shaposhnikov, JETP Lett. **44** (1986) 465, Nucl. Phys. B **287** (1987) 757, Nucl. Phys. B **299** (1988) 797;
   A.I. Bochkarev, S.Y. Khlebnikov and M.E. Shaposhnikov, Nucl. Phys. B **329** (1990) 490;
   L. McLerran, Phys. Rev. Lett. **62** (1989) 1075;
   L. McLerran, M.E. Shaposhnikov, N. Turov and M. Voloshin, Phys. Lett. **256** (1991) 451;
   N. Turov and P. Zadrozny, Nucl. Phys. B **358** (1991) 471;
   M. Dine, P. Huet, R. Singleton and L. Susskind, Phys. Lett. **257** (1991) 351;
   A. Cohen, D.B. Kaplan and A.E. Nelson, Nucl. Phys. B **349** (1991) 727, Phys. Lett. B **263** (1991) 86 and preprint UCSD-PTH-91-20 (1991).

7. S. Weinberg, Phys. Rev. Lett. **19** (1967) 1264; A. Salam, Elementary Particle Physics, ed. by N. Svartholm (Almquist and Wiksells, Stockholm 1968), p. 367.
8. M.B. Gavela, P. Hernandez, J. Orloff and O. Pene, Mod. Phys. Lett. A **9** (1994) 795.
9. K. Kleinknecht, these proceedings.
10. M. Kobayashi and T. Maskawa, Prog. Th. Phys. **49** (1973) 652;
N. Cabibbo, Phys. Rev. Lett. **10** (1963) 531.
11. L. Wolfenstein, Phys, Rev. Lett. **51** (1983) 1945.
12. C. Caso *et al*, Particle Data Group, Eur. Phys. Jour. C **3** (1998) 1.
13. M. Neubert, *B Physics and CP Violation*, preprint CERN–96–04, pag. 121. References therein.
14. T. Inami and C.S. Lim, Prog. Theor. Phys. **65** (1981) 297 and 1772.
A.J. Buras, Phys. Rev. Lett. **46** (1981) 1354.
A.J. Buras, M. Jamin and P.H. Weisz, Nucl. Phys. B **347** (1990) 491.
15. The *BABAR* Collaboration, *The BABAR Physics Book*, ed. P.F. Harrison and H.R. Quinn, October 1998, SLAC Report 504.
16. M. Gronau and D. Wyler, Phys. Lett. B **265** (1991) 172;
I. Dunietz, Phys. Lett. B **270** (1991) 75;
M. Gronau, J. Rosner and D. London, Phys. Rev. Lett. **73** (1994) 21.
17. A. Einstein, B. Podolsky and N. Rosen, Phys. Rev. D **47** 777 (1935).
18. K. Pitts, these proceedings.
19. P. Oddone, Proceedings of the UCLA Workshop: Linear Collider $B\overline{B}$ Factory Conceptual Design, ed. by D.Stock (1987);
G. Feldman *et al.*, preprint SLAC-PUB-4838, CNLS 89/884, LBL-26790, January 1989.
20. D. Boutigny *et al.*, The *BABAR* Collaboration, SLAC Report 457, March 1995.
21. M.T. Cheng *et al.*, The *BELLE* Collaboration, BELLE-TDR-3-95, March 1995.